A Search for Exoplanets around Northern Circumpolar Stars. IX. A Multi-Period Analysis of the M Giant HD 135438[†]

Byeong-Cheol Lee [iD][1,2] ⋆**, Jae-Rim Koo** [iD][3]**, Yeon-Ho Choi** [iD][1,2]**, Tae-Yang Bang**[4]**,
Beomdu Lim** [iD][3]**, Myeong-Gu Park** [iD][4]**, and Gwanghui Jeong**[5]

[1]Korea Astronomy and Space Science Institute, Daejeon 34055, Republic of Korea

[2]Korea National University of Science and Technology, Daejeon 34113, Republic of Korea

[3]Kongju National University, Gongju-si, Chungcheongnam-do 32588, Republic of Korea

[4]Department of Astronomy and Atmospheric Sciences, Kyungpook National University, Daegu 41566, Republic of Korea

[5]Space Science Research Center, Antbridge Inc, Daejeon 34120, Republic of Korea

⋆Corresponding Author: B.-C. Lee, bclee@kasi.re.kr

Abstract

It is difficult to distinguish the pure signal produced by an orbiting planetary companion around giant stars from other possible sources, such as stellar spots, pulsations, or certain activities. Since 2003, we have obtained radial (RV) data from evolved stars using the high-resolution, fiber-fed Bohyunsan Observatory Echelle Spectrograph (BOES) at the Bohyunsan Optical Astronomy Observatory (BOAO). Here, we report the results of RV variations in the binary star HD 135438. We found two significant periods: 494.98 d with eccentricity of 0.23 and 8494.1 d with eccentricity of 0.83. Considering orbital stability, it is impossible to have two companions in such close orbits with high eccentricity. To determine the nature of the changes in the RV variability, we analyzed indicators of stellar spot and stellar chromospheric activity to find that there are no signals related to the significant period of 494.98 d. However, we calculated the upper limits of rotation period of the rotational velocity and found this to be 478–536 d. One possible interpretation is that this may be closely related to the rotational modulation of an orbital inclination at 67–90 degrees. The other signal corresponding to the period of 8494.1 d is probably associated with a stellar companion orbiting the giant star. A Markov Chain Monte Carlo (MCMC) simulation considering a single companion indicates that HD 135438 system hosts a stellar companion with $0.57^{+0.017}_{-0.017}\ M_\odot$ with an orbital period of 8498 d.

Keywords: stars: individual: HD 135438 — techniques: radial velocities — stars: planetary systems

1. Introduction

As of September of 2023, approximately one hundred giant planets have been found around giant stars[1]. These giant planets are heavier than those found around solar-type stars. This can occur because huge stars are expected to have heavier planets compared to our Sun. In particular, identifying exoplanets around giant stars is quite tricky compared to exoplanet exploration, as various fluctuations of the activities from giants are observed in combination with pure RV from an orbital motion.

Furthermore, it is highly meaningful and rare in itself to find a substellar companion through radial velocity (RV) observations around red giant branch stars (RGB) and around asymptotic giant branch syars (AGB) that have a greatly expanded and active stellar atmosphere. In particular, the fact that substellar companions survived the RGB and AGB stages of Hertzsprung-Russell diagram presents another viable research topic related to planetary survival problems. Recently, Hon et al. (2023) conducted follow-up observations on the red giant 8 UMi (Baekdu[2]; Lee et al. 2015), an RGB-stage exoplanet system and showed that 8 UMi b (Halla[2]; Lee et al. 2015) survived the RGB phase and this may be expected to be the normal case. The system shows that core-helium-burning red giants can accommodate close planets, providing evidence that binarity plays a role in long-term survival of late exoplanets. Understanding the exoplanets around stars in their late evolutionary phase as in this study is certain to be one of the main topics in future studies of exoplanets.

Current knowledge pertaining to the evolutionary paths of evolved stars is insufficient to predict the fate of these systems. We need to understand the dynamics of planetary systems

---

[†]This work is based on the data obtained with the Bohyunsan Observatory Echelle Spectrograph (BOES).

[1]https://exoplanet.eu/

[2]https://www.nameexoworlds.iau.org/2019approved-names

Table 1. Stellar parameters for HD 135438.

Parameter	Value	Reference
Spectral type	K5	*HIPPARCOS* (Esa 1997)
	M0 III	This work
m_v (mag)	5.98	*HIPPARCOS* (Esa 1997)
$B-V$ (mag)	1.56	*HIPPARCOS* (Esa 1997)
$V-K$ (mag)	3.82	*HIPPARCOS* (Esa 1997)
π (mas)	4.92 ± 0.37	Gaia Collaboration et al. (2023)
$T_{\rm eff}$ (K)	$4,639^{+10.7}_{-3.4}$	Gaia Collaboration et al. (2023)
	$4,032 \pm 30$	This work
[Fe/H]	$-0.61^{+0.0003}_{-0.0009}$	Gaia Collaboration et al. (2023)
	-0.36 ± 0.08	This work
$\log g$ (cgs)	$1.73^{+0.015}_{-0.005}$	Gaia Collaboration et al. (2023)
	1.17 ± 0.14	This work
$v_{\rm micro}$ (km s^{-1})	1.77 ± 0.12	This work
$R_\star$ ($R_\odot$)	44.553	McDonald et al. (2017)
	50.15 ± 2.59	Kervella et al. (2022)
$M_\star$ ($M_\odot$)	1.59 ± 0.08	Kervella et al. (2022)
$L_\star$ ($L_\odot$)	396.325 ± 0.099	McDonald et al. (2017)
	734^{+37}_{-34}	Gaia Collaboration et al. (2023)
$v_{\rm rot} \sin i$ (km s^{-1})	4.72	This work
$P_{\rm rot}/\sin i$ (days)	$(478\text{--}538) \pm 30$	This work

Figure 1. The H−R diagram illustrating the property of HD 135438. Pairs of evolutionary tracks from (Girardi et al. 2000) for the star with 1.6 $M_\odot$, Z = 0.008 (solid line), 1.5 $M_\odot$, Z = 0.008 (dashed line), and 1.6 $M_\odot$, Z = 0.019 (dash dotted line). Asterisks show the helium flash point. Each star mark denotes the position of the star assuming a different radius.

around evolved giants. Also, the number of such evolved stars with planetary companion is limited. Future research will provide more candidates to enable better tracking of the form of companion mass functions and to understand the origin and history of such systems.

Since 2003, we have been searching for exoplanets using the RV technique based on homogeneous data sets from the same instrument. In this study, we report the HD 135438 system showing two significant periodic signals in RV variation. It is important to note that HD 135438 is known as a visual binary. Its companion (HIP 74567) is 118.2″ away from HD 135438 (Mason et al. 2001). However, these two stars have far different parallaxes (5.011 mas for HD 135438 and 2.1548 mas for HIP 74567) as well as proper motions (Gaia Collaboration et al. 2023). Therefore, this binary pair seems not to be gravitational bound, and the RV variations are not affected by their orbital motion. We investigate the origins of the RV variations seen only in HD 135438 using several methods. HD 135438 is listed in HIPPARCOS-Gaia Catalog of Accelerations (HGCA; Brandt 2018, 2021) showing a small variation of proper motion and Renormalized Unit Weight Error (RUWE) astrometric goodness-of-fit statistic in Gaia DR3 is 4.246, greater than nominal good range of 1.0–1.4 and indicates that unresolved companion is expected (Stassun & Torres 2021). Therefore, we could expect that HD 135438 is a system with at least stellar mass companion.

In Section 2, we describe our observations and the data reduction method. The stellar parameters of this star are addressed in Section 3. We analyze the periodogram and orbital stability in Section 4. In Section 5, we discuss a number of possible origins of the RV variations. In Section 6, we discuss the overall results of this study.
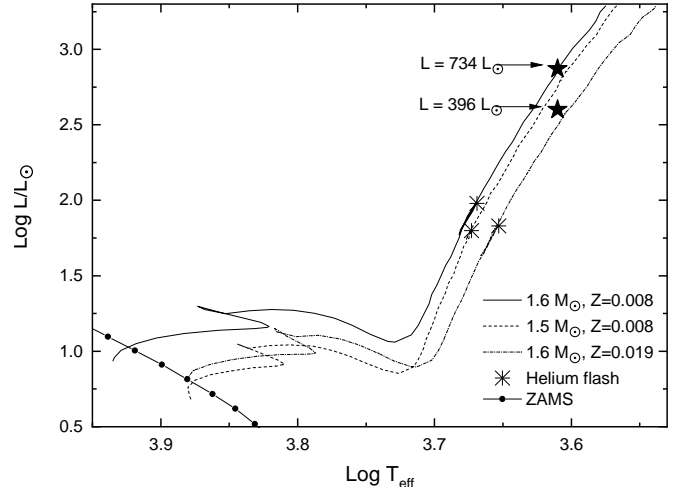
2. Observations and Data Reduction

We conducted the "**S**earch for **E**xoplanets around **N**orthern circumpolar **S**tars" (SENS; see Lee et al. 2015), which uses the fiber-fed high-resolution Bohyunsan Observatory Echelle Spectrograph (BOES) attached to the 1.8 m telescope at BOAO in Korea (Kim et al. 2007). Approximately 200 circumpolar stars were selected for the survey, of which 5% are dwarf stars, 40% are giant stars, and 55% are stars of an unclassified luminosity class covering all spectral types.

BOES is equipped with an iodine absorption (I$_2$) cell of the type needed for more precise RV measurements. Before starlight enters the fiber, it passes through the I$_2$ absorption cell regulated at 67 °C, which superimposes thousands of molecular absorption lines over the object spectra in the spectral region between 4,900 and 6,000 Å. We used a fiber with a diameter of 200 μm, which yields a resolving power outcome R = 45000. Total of 110 spectra were obtained for HD 135438 from January of 2009 to February of 2023. The measured signal-to-noise (S/N) ratio in the region of 5000 Å was approximately 100–200 with a typical exposure time ranging from 500 to 900 s. The RV standard star τ Ceti, monitored since 2003, was shown to maintain a stable RV value of 7.5 m s^{-1} for 20 years (Lee et al. 2013).

The standard reduction procedures of flat-fielding, scattered light subtraction, and order extraction from raw CCD images were carried out using the IRAF software package. Precise RV measurements related to the I$_2$ analysis were undertaken using RVI2CELL (Han et al. 2007), which is based on a method used in Valenti et al. (1995) and Butler et al. (1996). For the modeling of the instrument profile, we used the matrix formula described by Endl et al. (2000). The RV measurements for HD 135438 are listed in Table A.1.
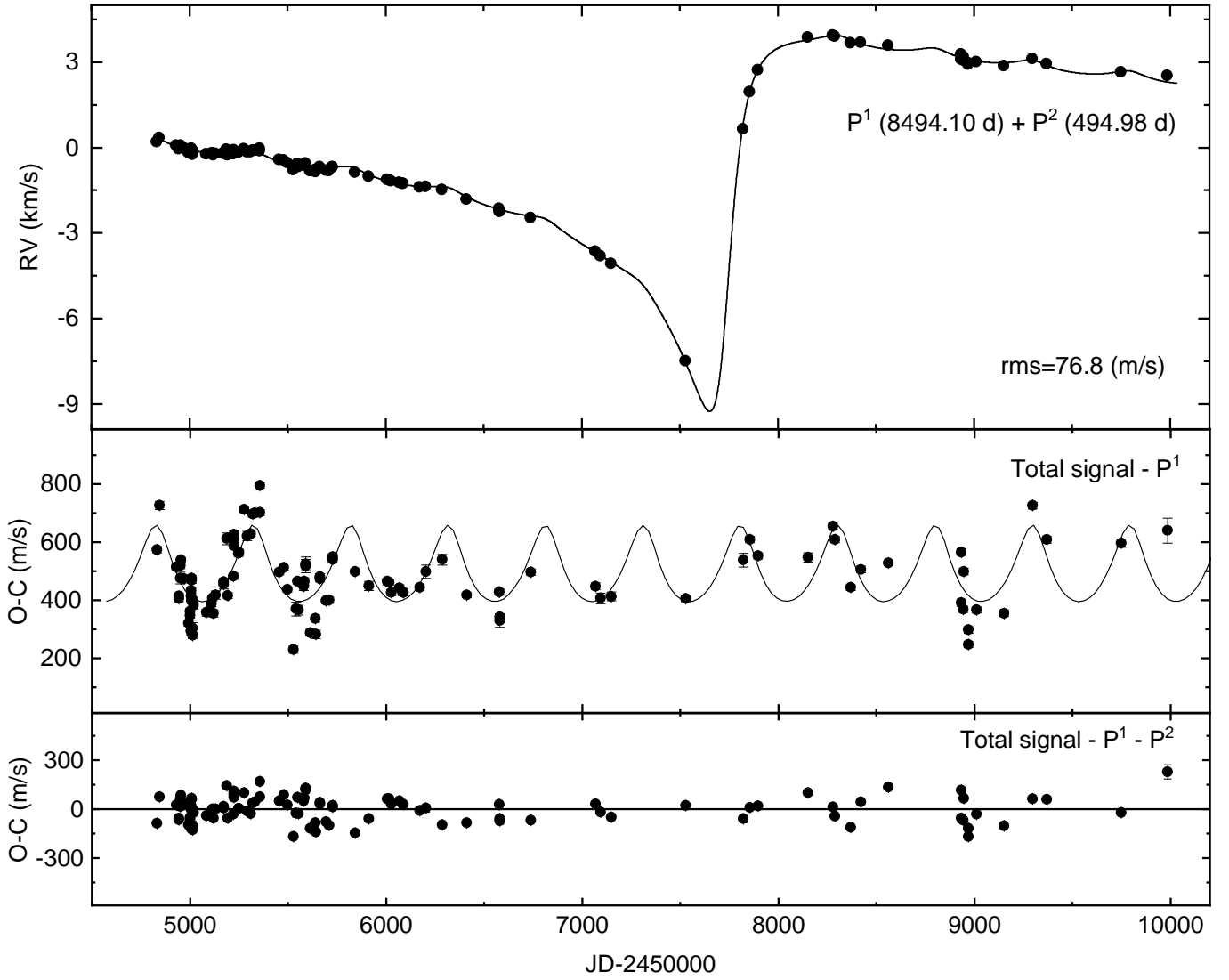
Figure 2. Orbital fit of HD 135438: (top panel) Kepler RV model with two companions, (middle panel) the residual RVs after subtracting the strong peak of 8494.10 d, and (bottom panel) residual RVs after subtracting the orbit with two strong periods.

3. Stellar Characteristics

3.1. Fundamental Parameters

The basic stellar parameters were based on the *HIPPARCOS* catalog (Esa 1997) and Gaia DR3 (Kervella et al. 2022; Gaia Collaboration et al. 2023). The stellar atmospheric parameters such as the temperature ($T_{\rm eff}$), metal abundance ([Fe/H]), surface gravity (log g), and micro turbulence ($v_{\rm micro}$) were determined from around 84 equivalent width (EW) measurements of Fe I and Fe II lines using TGVIT (Takeda et al. 2005), which is based on the Kurucz (1992) atmosphere models. This procedure usually requires three constraint conditions, the excitation equilibrium, ionization equilibrium, and the matching of the curve of the growth shape (Takeda et al. 2002).

The spectral type of HD 135438 has been classified as K5, while its luminosity class is still unknown (Esa 1997). The star could be classified as a giant according to the low surface gravity and large stellar radius values compared to those of dwarf stars. A *HIPPARCOS B−V* color index of approximately 1.56 and our estimation of $T_{\rm eff}$ indicate that the spectral type is close to an early M. The *V−K* color of 3.85 is also similar to that of M0 III (*V−K* = 3.85) in Bessell & Brett (1988). Accordingly, HD 135438 should be an early M giant star. Because the stellar radius is the major factor determining the fate of companions in the evolutionary track of giant stars, we quoted two values provided in recent studies (McDonald et al. 2017; Kervella et al. 2022). The basic stellar parameters are summarized in Table 1.

3.2. Stellar Properties

Figure 1 shows HD 135438 in a H-R diagram along with its theoretical evolution track (Girardi et al. 2000). We plot the evolutionary tracks of 1.5 $M_\odot$ and 1.6 $M_\odot$ stars for Z = 0.008 and Z = 0.019 in the diagram. The star is located at the AGB stage on the H-R diagram after having undergone a helium flash, leaving at giant clump. The fate of their companions when they interact with the atmospheres of the expanding host stars is unclear. Therefore, an exoplanet search around stars at the AGB stage is of great significance in understanding the fate of the planet in each case.
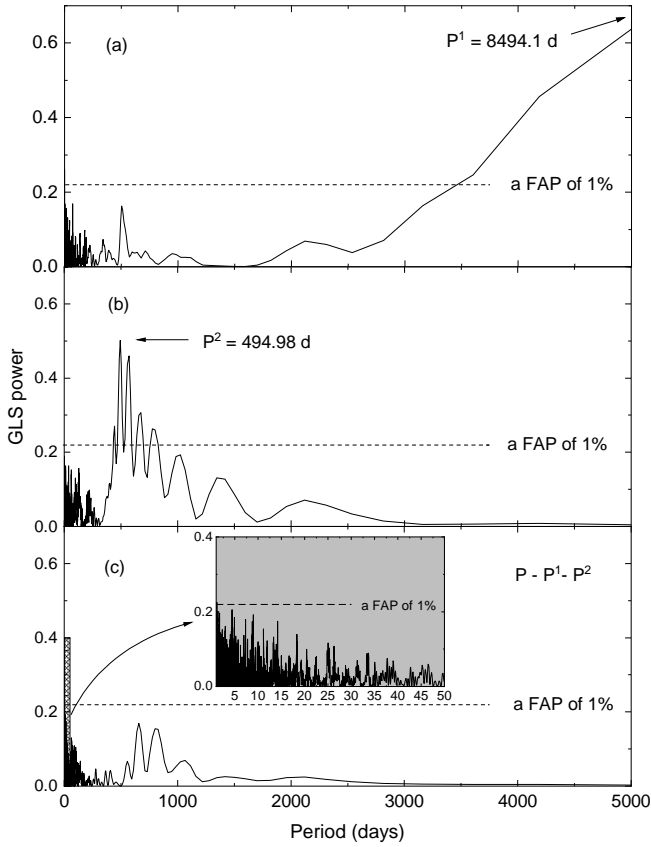
Figure 3. GLS periodograms for RVs of HD 135438. (a) GLS periodogram for RVs of HD 135438, (b) The same periodogram for the residual RVs after subtracting the strong peak of 8494.10 d, (c) periodogram of the residual RVs after subtracting two strong peaks. A square gray box denotes the range of the short period in which the RVs were measured. The horizontal lines in each panel correspond to a 1% FAP.

4. Orbital Solutions

We used RVI2CELL (Han et al. 2007) for the best fit to determine the orbital parameters. In order to determine the periodicity in the BOES RV variations, we used the Generalized Lomb-Scargle periodogram (GLS; Zechmeister & Kürster 2009). GLS provides more accurate frequencies and determines the spectrum intensity less sensitive to aliasing.

The RV measurements of HD 135438 as a function of the Julian Date are shown in Figure 2. GLS periodogram reveals the presence of a clear 494.98 d period signal in addition to the long-term variation of a period of 8494.1 d (Figure 3). In other words, we initially subtracted a significant cycle of 8494.1 d, and then repeated pre-whitening procedures of (Blomme et al. 2011) to find additional variability in the residuals (Figure 3). Figure 4 shows the phase-folded curve of 494.98 d and the residual around the solution is 76.8 m s^{-1}. The GLS false-alarm probability (FAP) was calculated using a bootstrap randomization process (Kürster et al. 2003). The RV data were shuffled 200,000 times keeping the times fixed.

We performed all analyses using the Markov Chain Monte Carlo (MCMC) algorithm and Exo-Striker (Trifonov 2019) to evaluate the error of the parameters and to fit the data more
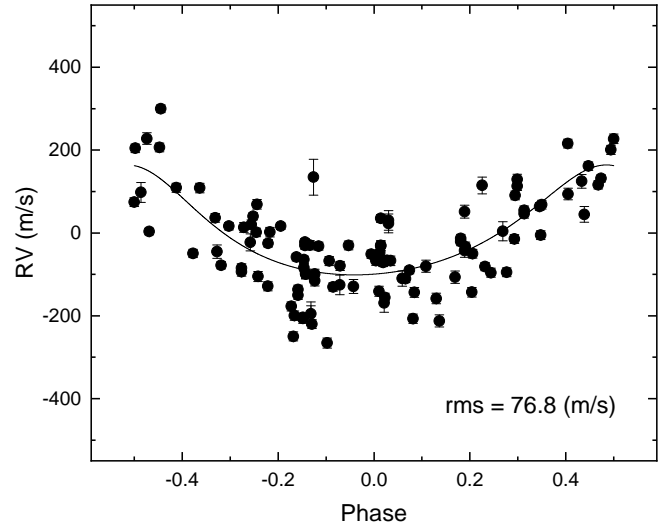

Figure 4. Phase-folded curve of the 494.98 d with points representing the observed RVs for HD 135438. It is displayed after a subtraction the signal of P = 8494.1 d and after removing the effect of the decreasing trend.

Table 2. Orbital solutions for short period and long period probed by the MCMC simulation.

parameter	P2 (short period)	P1 (long period)
P (days)	$494.98^{+1.65}_{-3.86}$	$8{,}494.10^{+0.87}_{-3.0}$
K (m s^{-1})	$139.1^{+3.1}_{-0.9}$	$6{,}452.7^{+2.8}_{-10.0}$
e	$0.23^{+0.06}_{-0.08}$	$0.83^{+0.00}_{-0.00}$
$T_{\text{periastron}}$ (JD)	$2{,}454{,}359.619^{+70}_{-65}$	$2{,}449{,}234.881^{+50}_{-27}$
ω (deg)	$24.28^{+0.48}_{-1.27}$	$235.31^{+0.33}_{-0.24}$
$m \sin i$ (M_J)	$7.21^{+0.32}_{-0.30}$	$599.51^{+16.93}_{-19.06}$
a (au)	$1.43^{+0.02}_{-0.02}$	$10.54^{+0.15}_{-0.17}$
Slope (m s^{-1} d^{-1})	$-0.0012^{+0.0040}_{-0.0029}$	
RV offset (m s^{-1})	$487.8^{+3.1}_{-1.2}$	
RV jitter (m s^{-1})	$27.86^{+6.38}_{-2.20}$	
N_{obs}	110	
rms (m s^{-1})	76.8	

robustly. The best-fit orbital parameters of the planetary signals in the final MCMC model are listed in Table 2. Two derived orbital parameters of the system are orbital periods of $494.98^{+1.65}_{-3.86}$ d and $8494.10^{+0.87}_{-3.0}$ d. The short period has a semi-amplitude of 139.1 m s^{-1} and eccentricity of 0.23 and the long period shows a semi-amplitude of 6452.7 m s^{-1} and eccentricity of 0.83.

4.1. Orbital Stability

The hierarchical triple system (two stellar one potential planet) of HD 135438 hosting two close companions with high eccentricities seems to be dynamically unstable. In order for planetary parameter estimation to be completed, a stability analysis must also be performed. The best-fit parameters should not only be the most likely parameter in the posterior analysis, but should also be stable for long enough time.

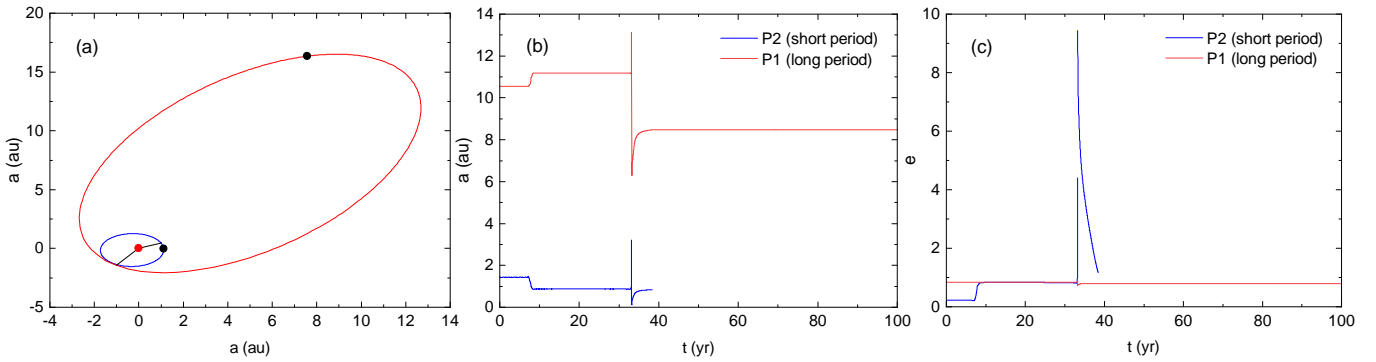The two eccentric companion's orbits of HD 135438 sys-

Figure 5. Orbital evolution of the HD 135438 system for a 100 yr extent for the best-fit orbit. (a) orbital fit, (b) the evolution of the semi-major axes, and (c) the eccentricities (blue color indicates the inner, red color the outer companion). See the text for details.

tems are likely to interact strongly with each other. We performed simple numerical orbital evolution simulations to test this possibility and study the system's dynamical architecture. We use a custom version of the SYMBA symplectic N-body algorithm (Duncan et al. 1998) integrated in the Exo-Striker toolbox (Trifonov 2019), which directly adopts and integrates the Jacobi orbital elements from the posterior orbital analysis. We tested the stability of the system up to 100 yr with a small time step of 0.2 days for 5000 randomly chosen samples from the orbital parameter posteriors.

Based on the best-fit orbital elements, especially semi-major axes and two eccentricities could be readily identifiable as a dynamically unstable system (e.g., Correia et al. 2016; Hamers et al. 2016; Busetti et al. 2018). Figure 5 shows the evolution of two orbits of P2 (short period) and P1 (long period). Simulations showed that the orbits were disrupted in just 35 yr [Figure 5(b)] and the eccentricity become unstable in less than ten years [Figure 5(c)]. In other words, HD 135438 cannot have two companions with such orbital parameters.

5. Origin of the RV Variations

The long-period RV variations in giants are, in general, related to various causes (i.e. stellar rotation, pulsation, and/or reflex orbital motion due to a companion). To uncover the origin of the detected RV variations, we studied four types of rotation modulations by spot indicators and four forms of chromospheric activity indicators for HD 135438.

5.1. Rotation Modulations by Spot Indicators

Stellar rotational modulation by inhomogeneous surface features can create variable asymmetries in spectral line profiles (Queloz et al. 2001). First, two bisector quantities were calculated from the line profiles at two flux levels (40% and 80%): the bisector velocity span BVS and the bisector velocity curvature BVC. No significant peak was found in the BVC measurements. In addition, the BVS measurements show strong signals in periods of ~50 d and ~200 d [Figure 6(b)]. However, they are not related to the periods found in the RV.

Second, variations in *HIPPARCOS* photometric data were analyzed. For three years, between JD 2447864.34722 (December 1989) and JD 2449061.91245 (March 1993), the *HIP-*

PARCOS satellite obtained 283 photometric measurements with an rms scatter of 0.011 mag, corresponding to 0.18% of variation. Figure 6(c) shows the GLS periodogram of these measurements. There is no significant peak.

Almost simultaneously, between JD 2447875 and JD 2449170, HD 135438 was observed in the near-infrared (NIR) 2.2 μ bands by NASA's *COBE* (Cosmic Background Explorer) satellite with the *DIRBE* (Diffuse Infrared Background Experiment) instrument. The total number of 80 weekly averaged fluxes in each band were extracted for HD 135438 from the *COBE/DIRBE* archives (Price et al. 2010). A GLS periodogram analysis of the 2.2 μ flux revealed a significant signal of 349.8 d in the domain of interest [Figure 6(d)].

In addition, we analyzed 18461 TESS data obtained for about 710 d for HD 135438. TESS data are available for 3 sectors and show about 2% differences between the sectors. An analysis of TESS data showed a peak of 4.56 d regardless of the rotational period and RV of HD 135438. However, it is well-known that there are flux jumps or offsets between TESS sectors. Moreover, the time span of TESS is much shorter than our orbital period of about 8500 d.

5.2. Rotation Modulations by Chromospheric Activity Indicators

Frequently used optical chromospheric activity indicators are the EW variations of Ca II H & K, H$_\beta$, Mg I b triplet, He I D$_3$, Na D$_1$ & D$_2$, H$_\alpha$, and Ca II infrared triplet (IRT) lines. The behaviors of the different optical chromospheric activity indicators reflect the atmospheric condition at different atmospheric heights: Na D$_1$ & D$_2$ and the Mg I b triplet for the upper photosphere and lower chromosphere (Basri et al. 1989; Andretta et al. 1997), Ca II IRT lines for the lower chromosphere (Martínez-Arnáiz et al. 2011), H$_\alpha$, H$_\beta$ and Ca II H & K for the middle chromosphere (Noyes et al. 1984; Montes et al. 1997) and He I D$_3$ for the upper chromosphere (Zirin 1988). We used four types of indicators to assess the chromospheric activities.

The emission of Ca II H cores is formed in the chromosphere and the chromospheric activity (Saar & Donahue 1997) shows a typical center reversal. Further emission from the center of the line suggests that the source function of the layer is greater than that of the light sphere. This reversal is common
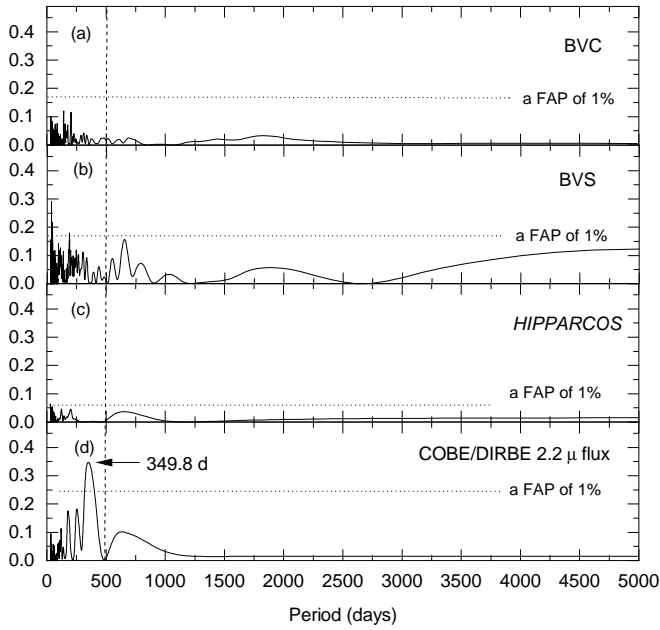
Figure 6. The GLS periodogram of the four kinds of spot indicators for HD 135438. (a) periodogram of the line bisector curvature (BVC), (b) the line bisector span (BVS), (c) periodogram of the HIPPARCOS photometric data, and (d) the COBE/DIRBE satelite 2.2 micro flux intensity measurement. The vertical dashed line indicates the period of 494.98 d.
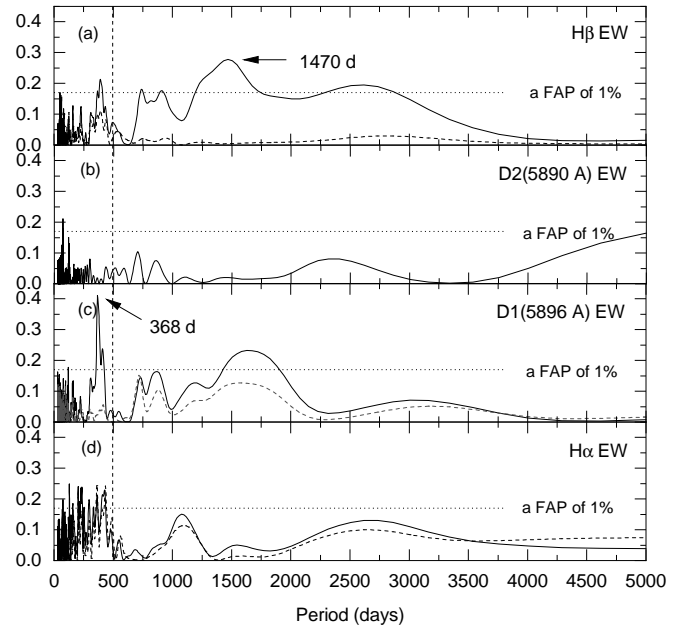

Figure 7. The GLS periodogram of the four kinds of Chromospheric activity indicators for HD 135438 (Short to long wavelength order). (a) periodogram of the H_β line EW variation, (b) periodogram of the sodium D_2 line EW variation, (c) periodogram of the sodium D_1 line EW variation, and (d) periodogram of the H_α line EW variation. The dashed lines in each panel mean periodogram of the residual after subtracting a strong peak. The horizontal line in each panel corresponds to a 0.1% FAP. The vertical dashed line indicates the location of the period of 494.98 days.

in cool stars and is closely linked to the convective sheath and magnetic activity. Unfortunately, the Ca II H & K line region for HD 135438 obtained by BOES has an insufficient S/N ratio, and the EW variation could not be estimated. Another Ca II indicator, the Ca II IRT lines is not suitable because our CCD spectra is saturated at wavelengths longer than approximately 6800 Å. Mg I b triplet lines are also excluded from the study because they are located inside the I_2 molecular region.

The H_α EW is believed to have a strong correlation with the Ca II index and is sensitive to the corresponding atmospheric stellar activity (Kürster et al. 2003). Owing to sparse blending lines, a weak telluric line, and a narrow H_α absorption line, it is easy to estimate the H_α EW. The H_β absorption line, which originates from the middle layers of stellar atmosphere and is sensitive to the stellar activity, was also measured. We measured the EWs using a band pass of ± 1.0 Å for H_α and ± 0.8 Å for H_β centered on the core of the lines to avoid nearby blending lines and ATM H_2O absorption lines (i.e. Ti I 6561.3, Na II 6563.9, and ATM H_2O 6564.0 Å). The GLS periodogram of the H_α and H_β EW variations is shown in Figure 7. The H_β periodogram shows high power at $\sim$1470 d, far from the RV period of 494.98 d.

We measured the sodium D lines at 5889.951 Å and 5895.924 Å using a band pass value of ± 0.5 Å centered at the core of the sodium lines. There is a large peak at a period of 368 days in the Na D_1 line [Figure 7(c)].

5.3. Pulsation

Evolved stars exhibit stellar spots and surface activities as well as pulsation, resulting in low amplitude RV fluctuations on

different time scales. Short-term ($\sim$days) RV variations are known to stem from stellar pulsations (Hatzes & Cochran 1998) and long-term (hundreds of days) RV variations with low-amplitudes can be caused by stellar pulsations, rotational modulations by uneven surface features, or planetary companions.

We estimated the fundamental periods, i.e., radial pulsation periods, and the expected amplitude using relationships devised by Kjeldsen & Bedding (1995). The radial pulsation period and the expected amplitudes were estimated: a pulsation RV amplitude of 58.3 m s^{-1}, a pulsation period of 5.7 d, and a fundamental period of 20.3 d. The periods are far too short to explain the RV variations we observed. Furthermore, we expect the pulsation RV amplitude of 58.3 m s^{-1} below the dispersion of 139.1 m s^{-1} measured for HD 135438.

5.4. Rotation Period

As stars evolve away from the MS, they become cooler and rotate more slowly. Low-amplitude and long-period RV variations in evolved stars may arise from the rotational modulation of surface features such as stellar spots (Lee, Mkrtichian, Han, Park, & Kim 2008; Lee, Han, Park, Kim, & Mkrtichian 2012). The rotation period of evolved stars is very important in distinguishing RV variations from the orbital motion from the rotational modulations. Lee et al. (2012) showed that low-amplitude and long-period RV variations can arise from the rotational motion in α Per. To estimate the stellar projected

Table 3. Orbital solutions for HD 135438 B probed by the MCMC simulation.

parameter	HD 135438 B
P (days)	$8{,}498.09^{+11.46}_{-3.58}$
K (m s^{-1})	$6{,}477.5^{+5.1}_{-14.8}$
e	$0.83^{+0.00}_{-0.00}$
$T_{\mathrm{periastron}}$ (JD)	$2{,}449{,}544.725^{+40}_{-30}$
ω (deg)	$235.0^{+0.5}_{-0.5}$
MA_b (deg)	$237.6^{+0.3}_{-0.2}$
λ_b (deg)	$112.7^{+0.36}_{-0.34}$
$m \sin i$ ($M_\odot$)	$0.57^{+0.017}_{-0.017}$
a (au)	$10.54^{+0.15}_{-0.15}$
Slope (m s^{-1} d^{-1})	$-0.0053^{+0.0080}_{-0.0078}$
RV offset (m s^{-1})	$488.1^{+4.2}_{-11.9}$
RV jitter (m s^{-1})	$91.1^{+17.8}_{-6.9}$
N_{obs}	110
rms (m s^{-1})	112.4

rotational velocity, we used a line-broadening model (Takeda et al. 2008). The observed stellar spectrum was convolved by an intrinsic spectrum model and a total macrobroadening function. The intrinsic spectrum model can be computed if a model atmosphere, v_{micro}, and the elemental abundance are given. These broaden spectral lines without altering their EW. Distinguishing between the broadening components is difficult for spectra of slowly rotating late-type stars because all of these have similar intrinsic line width profiles.

Regarding the actual determination of line broadening, we used the automatic spectrum-fitting technique (Takeda 1995) at a wavelength of 6080–6089 Å. This involves use of seven free parameters that specify the best fitting solution. In this study, the abundances of three elements (Ti, Fe, and Ni) showing sufficient values in the selected section were selected.

We estimated the minimum rotational velocities of 4.72 km s^{-1} for HD 135438. Based on the rotational speed and two stellar radii presented in the literature, we derived the upper limits of rotational periods of HD 135438 as follows.

$$P_{\mathrm{rot}} = 2\pi R_\star / [v_{\mathrm{rot}} \sin(i)] = (478\text{–}538) \pm 30 \text{ d} \quad (1)$$

6. Discussion

From literature and our new estimation of stellar parameters, HD 135438 was newly classified as an M0 giant (III) star, modified from a spectral type of K5. We observed HD 135438 using BOES for 14 years from 2009 to 2023 and detected two clear periodic signals in RV variations. The best Keplerian fit and MCMC simulation yield an orbital period of $494.98^{+1.65}_{-3.86}$ d, a semi-amplitude of $139.1^{+3.1}_{-0.9}$ m s^{-1}, and an eccentricity of $0.23^{+0.06}_{-0.08}$ and another orbital period of $8494.10^{+0.87}_{-3.0}$ d, a semi-amplitude of $6452.7^{+2.8}_{-10.0}$ m s^{-1}, and an eccentricity of $0.83^{+0.00}_{-0.00}$. Orbit stability tests indicated that if the HD 135438 system has two such companions and it is physically unstable.

Generally, most giants have intrinsic RV variations and exhibit pulsations and/or surface activities. To determine the cause of RV 494.98 d, all relevant analyses must be considered

comprehensively. DIRBE/COBE and Na D_2 measurements show periods of $\sim$350 d, though this does not appear to be related to the RV period of 494.98 d. Robust short periods in H_α EW have also been found, suggesting a possible pulsation of the star. The H_β EW period of 1,470 d can be suspected to be a triple of the RV variation of 494.98 d or the upper limits of rotation period of 478–538 d.

There are several ways to interpret the period of 494.98 d seen in RV variations. First, 498.98 d may actually be a harmonization of the actual one third of the 1,470 d period found in the H_β EW measurement. However, no significant cycle similar to H_β was found in chromospheric indicators other than H_β, and the relationship between the RV cycle and the chromospheric period corresponding to three times that cannot be explained scientifically. Second, the short-period variability may undoubtedly be due to radial and/or non-radial pulsation. However, long-period variability can still be interpreted as a viable hypothesis, stemming from rotational modulation caused by stellar pulsation. Proof of long-term pulsation is practically impossible in planetary exploration studies around giant stars and remains as an area for further study (Lee et al. 2008). Long-term pulsation of the M giant HD 135438 is also not substantially proven. In addition, many planets found around giant stars also have eccentricities above 0.2[3]. This may mean that such eccentric modulation of HD 135438 is difficult to be produced by surface variations or stellar pulsation. Finally, the 494.98 d period may actually be the rotation period of the star. The variation is strongly suspected to be due to the rotational period, if the rotational modulations are due to an orbital inclination at 67–90 degrees. Although the mechanism generating such low amplitude, long-period pulsation modes is not well understood, we speculate that the current RV fluctuations seen in HD 135438 are more likely to be the result of the rotational period as opposed to the stellar pulsation.

Figure B.1 shows the posterior distributions of the parameters sampled from the model MCMC with one companion. The best-fit orbital parameters of the companion signal in the final MCMC model are listed in Table 3. Thus, the period of 8498.09 d is judged to be due to a stellar companion with a minimum companion mass of $0.57^{+0.017}_{-0.017} M_\odot$ and with a semi-major axis of $10.54^{+0.15}_{-0.15}$ au. Even if the simulation was set to one million years, it remained stable. Our analyses show that for HD 135438, the long-term variation is caused by a stellar companion and the short-term variation can be attributed to the rotational modulation. In this study, HD 135438 is thus classified a single-lined spectroscopic binary star.

---

[3] https://exoplanet.eu/

References

Andretta, V., Doyle, J. G., & Byrne, P. B. 1997, A&A, 322, 266

Basri, G., Wilcots, E., & Stout, N. 1989, PASP, 101, 528

Bessell, M. S., & Brett, J. M. 1988, PASP, 100, 1134

Blomme, R., Mahy, L., Catala, C., et al. 2011, A&A, 533, A4

Brandt, T. D. 2018, ApJS, 239, 31

Brandt, T. D. 2021, ApJS, 254, 42

Busetti, F., Beust, H., & Harley, C. 2018, in AAS Meet. Abstr., Vol. 232, 111.01

Butler, R. P., Marcy, G. W., Williams, E., et al. 1996, PASP, 108, 500

Correia, A. C. M., Boué, G., & Laskar, J. 2016, Celest. Mech. Dyn. Astron., 126, 189

Duncan, M. J., Levison, H. F., & Lee, M. H. 1998, AJ, 116, 2067

Endl, M., Kürster, M., & Els, S. 2000, A&A, 362, 585

Esa, . 1997, VizieR Online Data Catalog, I/239

Gaia Collaboration, Vallenari, A., Brown, A. G. A., et al. 2023, A&A, 674, A1

Girardi, L., Bressan, A., Bertelli, G., & Chiosi, C. 2000, A&AS, 141, 371

Hamers, A. S., Perets, H. B., & Portegies Zwart, S. F. 2016, MNRAS, 455, 3180

Han, I., Kim, K.-M., Byeong-Cheol, L., & Valyavin, G. 2007, Publ. Korean Astron. Soc., 22, 75

Hatzes, A. P., & Cochran, W. D. 1998, MNRAS, 293, 469

Hon, M., Huber, D., Rui, N. Z., et al. 2023, Nature, 618, 917

Kervella, P., Arenou, F., & Thévenin, F. 2022, A&A, 657, A7

Kim, K.-M., Han, I., Valyavin, G. G., et al. 2007, PASP, 119, 1052

Kjeldsen, H., & Bedding, T. R. 1995, A&A, 293, 87

Kürster, M., Endl, M., Rouesnel, F., et al. 2003, A&A, 403, 1077

Kurucz, R. L. 1992, in The Stellar Populations of Galaxies, ed. B. Barbuy & A. Renzini, Vol. 149, 225

Lee, B.-C., Han, I., & Park, M.-G. 2013, A&A, 549, A2

Lee, B.-C., Han, I., Park, M.-G., Kim, K.-M., & Mkrtichian, D. E. 2012, A&A, 543, A37

Lee, B.-C., Mkrtichian, D. E., Han, I., Park, M.-G., & Kim, K.-M. 2008, AJ, 135, 2240

Lee, B.-C., Park, M.-G., Lee, S.-M., et al. 2015, A&A, 584, A79

Martínez-Arnáiz, R., López-Santiago, J., Crespo-Chacón, I., & Montes, D. 2011, MNRAS, 414, 2629

Mason, B. D., Wycoff, G. L., Hartkopf, W. I., Douglass, G. G., & Worley, C. E. 2001, AJ, 122, 3466

McDonald, I., Zijlstra, A. A., & Watson, R. A. 2017, MNRAS, 471, 770

Montes, D., Fernandez-Figueroa, M. J., de Castro, E., & Sanz-Forcada, J. 1997, A&AS, 125, 263

Noyes, R. W., Hartmann, L. W., Baliunas, S. L., Duncan, D. K., & Vaughan, A. H. 1984, ApJ, 279, 763

Price, S. D., Smith, B. J., Kuchar, T. A., Mizuno, D. R., & Kraemer, K. E. 2010, ApJS, 190, 203

Queloz, D., Henry, G. W., Sivan, J. P., et al. 2001, A&A, 379, 279

Saar, S. H., & Donahue, R. A. 1997, ApJ, 485, 319

Stassun, K. G., & Torres, G. 2021, ApJ, 907, L33

Takeda, Y. 1995, PASJ, 47, 287

Takeda, Y., Ohkubo, M., & Sadakane, K. 2002, PASJ, 54, 451

Takeda, Y., Ohkubo, M., Sato, B., Kambe, E., & Sadakane, K. 2005, PASJ, 57, 27

Takeda, Y., Sato, B., & Murata, D. 2008, PASJ, 60, 781

Trifonov, T. 2019, The Exo-Striker: Transit and radial velocity interactive fitting tool for orbital analysis and N-body simulations, Astrophysics Source Code Library, ascl:1906.004

Valenti, J. A., Butler, R. P., & Marcy, G. W. 1995, PASP, 107, 966

Zechmeister, M., & Kürster, M. 2009, A&A, 496, 577

Zirin, H. 1988, Astrophysics of the sun (Cambridge University Press)

Appendix A. RV Measurements

In this appendix we present all observational data collected with the BOES. We list the observation dates Julian date (JD), the radial velocities (RV), and uncertainly ($\pm\sigma$), respective.

Table A.1. RV measurements for HD 135438 from January of 2009 to February of 2023 using the BOES.

JD [$-2,450,000$]	RV [m s^{-1}]	$\pm\sigma$ [m s^{-1}]	JD [$-2,450,000$]	RV [m s^{-1}]	$\pm\sigma$ [m s^{-1}]	JD [$-2,450,000$]	RV [m s^{-1}]	$\pm\sigma$ [m s^{-1}]
4833.402507	213.6	10.6	5225.409433	−91.7	10.5	6085.242850	−1261.7	12.2
4846.366796	356.4	14.1	5248.251809	−162.3	9.4	6089.001474	−1267.7	11.4
4930.297545	74.6	9.1	5250.391613	−159.9	10.6	6173.022731	−1377.0	10.6
4943.213495	−46.0	11.0	5277.164873	−38.1	10.6	6203.920031	−1370.9	23.2
4943.228113	−37.3	10.2	5291.350141	−142.6	16.4	6287.341771	−1466.3	19.2
4952.055646	17.2	20.3	5311.076286	−154.6	8.6	6412.264790	−1811.0	9.0
4953.085905	59.4	10.9	5321.069117	−95.6	10.8	6577.899414	−2140.3	10.4
4955.055031	77.4	8.7	5330.969083	−101.5	10.3	6577.910711	−2139.4	10.4
4970.206467	−0.7	9.0	5355.973046	−124.0	10.5	6578.926794	−2240.2	22.8
4994.032628	−173.6	10.6	5357.171521	−32.0	9.3	6579.900646	−2229.8	10.7
5000.972763	−138.8	10.2	5454.925105	−428.7	10.2	6739.203884	−2463.5	10.6
5000.981895	−152.6	9.7	5479.915571	−439.7	7.7	7067.216176	−3635.4	11.4
5006.047602	−212.8	11.9	5495.892147	−531.2	9.1	7094.162059	−3800.1	18.4
5006.062404	−210.8	10.4	5527.396061	−771.8	12.0	7148.279110	−4061.5	14.9
5006.989215	−91.2	9.6	5540.409972	−645.2	23.7	7527.220574	−7486.8	10.9
5007.000661	−72.0	9.0	5549.405862	−559.9	10.7	7820.143822	658.7	23.7
5008.008532	−30.6	9.0	5554.408807	−664.1	16.6	7856.136497	1964.0	10.9
5008.019353	−38.3	9.5	5581.270083	−611.6	14.1	7896.172874	2732.5	10.7
5008.986774	−107.9	11.1	5582.308892	−595.5	11.8	8151.224361	3876.6	15.7
5008.997607	−108.5	12.0	5582.323303	−596.9	11.6	8278.039731	3951.5	10.4
5014.071022	−208.8	28.6	5590.274493	−551.1	22.8	8288.005190	3900.1	10.1
5014.088799	−208.5	19.2	5590.291126	−544.0	23.6	8369.992102	3674.6	9.8
5015.102777	−234.6	10.8	5615.290706	−808.3	11.2	8421.885834	3693.4	12.0
5018.040687	−116.6	12.0	5639.198086	−786.4	12.7	8562.246191	3586.3	9.5
5018.133470	−132.8	12.2	5642.353973	−844.0	14.5	8932.127325	3277.3	11.5
5083.945047	−216.0	11.9	5664.254616	−670.0	9.9	8933.134096	3102.5	12.0
5110.910930	−210.0	9.2	5664.260647	−677.4	9.8	8943.311670	3069.9	10.9
5114.913916	−193.0	8.8	5695.029390	−787.6	10.9	8945.293022	3198.8	11.6
5119.902543	−251.1	11.8	5711.256563	−805.3	10.7	8969.291772	2925.7	10.8
5131.903171	−198.7	14.4	5728.992361	−676.9	10.7	8970.291164	2975.1	11.2
5171.373692	−197.2	16.3	5729.006990	−684.6	10.5	9009.985391	3009.6	10.0
5172.381133	−188.9	11.2	5841.928544	−864.5	8.2	9151.877273	2875.8	11.7
5189.389995	−56.2	20.2	5911.390040	−1001.4	16.1	9297.093635	3127.2	11.4
5192.390103	−255.3	9.9	6006.353462	−1113.1	11.1	9370.216577	2950.7	11.5
5222.401635	−216.6	10.5	6015.368679	−1127.8	9.4	9747.092776	2654.5	14.1
5223.276255	−112.1	10.6	6026.110672	−1178.7	10.9	9983.214549	2530.8	43.3
5225.236967	−75.1	12.3	6069.300772	−1223.7	10.0	—	—	—

Appendix B. Corner Plot

We present the posterior distributions of the parameters sampled from the model MCMC fit.
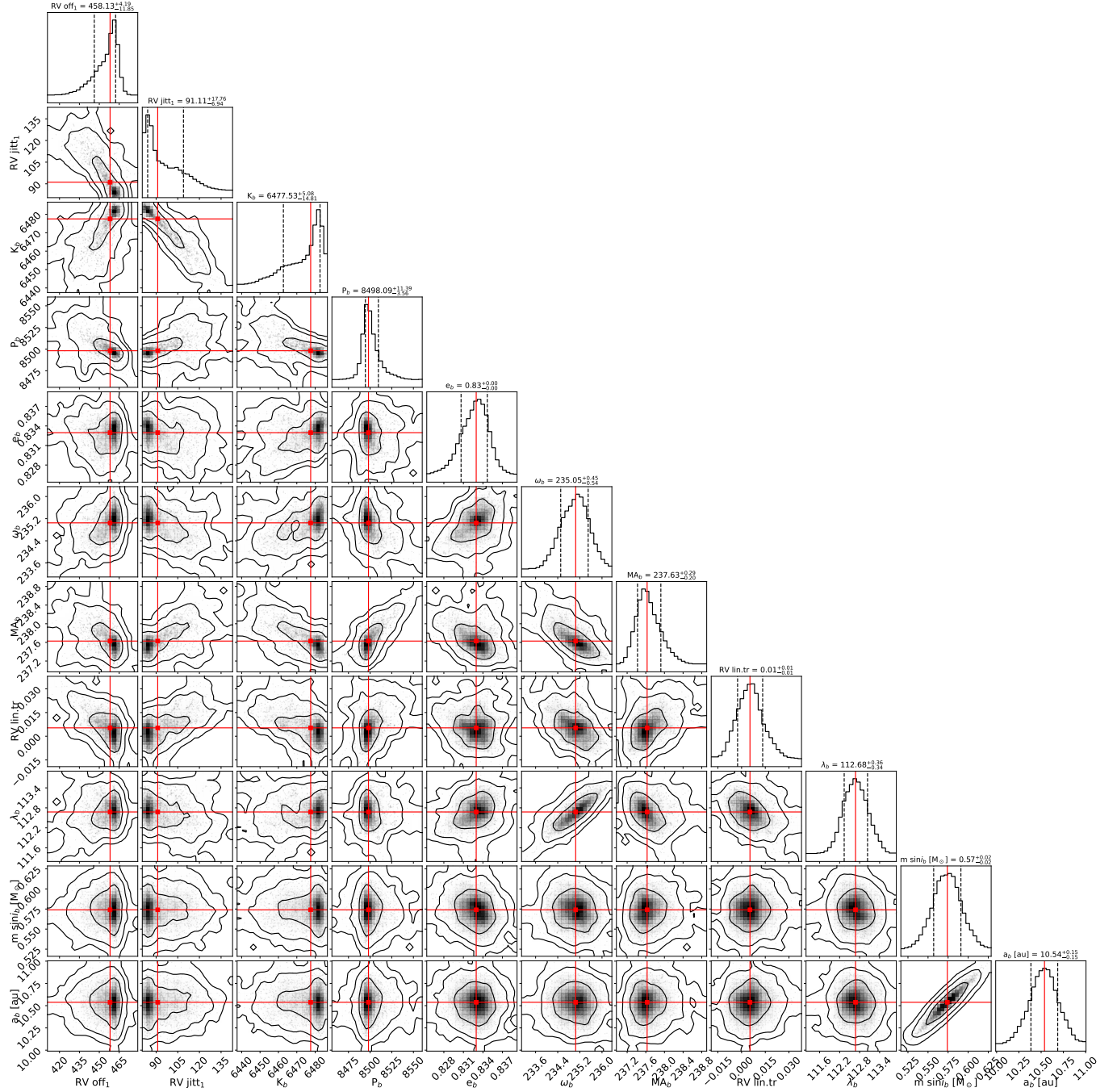

Figure B.1. Corner plot from the MCMC analysis on the corrected RV time-series showing the posterior distributions of the main internal structure parameters of HD 135438 B. The titles of each column correspond to the median and $1\,\sigma$, which are also shown with the dashed lines. This analysis involves fitting a model that consists of an offset, an RV jitter, the semi-amplitude (K_b), the orbital period (P_b), orbital eccentricity (e_b), periastron angle (ω_b), mean anomaly (MA_b), Slope (RV lin.tr), mean longitude λ_b, minimum mass ($m\sin i$), and Semi-major axis (a_b), respectively.